Interplay between homogeneous and heterogeneous electrocatalytic mechanisms determines the selectivity of the copper-catalyzed ammonia oxidation to nitrite and nitrate

Sam Johnston[†,‡], Liam Kemp[†§], Bila Turay[†▽], Alexandr N. Simonov[†,‡,], Bryan H. R. Suryanto[†,*], Douglas R. MacFarlane[†,‡]*

[†] School of Chemistry and the [‡]ARC Centre of Excellence for Electromaterials Science, Monash University, Clayton, VIC 3800, Australia

[§] School of Chemistry, University of Southampton, Southampton, SO17 1BJ, UK

[▽] Department of Chemistry, University of Warwick, Coventry, CV4 7AL, UK

Abstract

Electrocatalytic oxidation of ammonia is an appealing low-temperature process for the production of nitrites and nitrates that avoids the formation of pernicious N_2O and can be fully powered by renewable electricity, but the number of known efficient catalysts for such a reaction is limited at present. The present work demonstrates that copper-based electrodes exhibit high electrocatalytic activity and selectivity for the NH_3 oxidation to NO_2^-/NO_3^- in alkaline solutions. Systematic investigation of the effects of pH and potential on the kinetics of the reaction using voltammetric analysis and *in situ* Raman spectroscopy suggests that ammonia electrooxidation on copper occurs *via* two primary catalytic mechanisms. The first converts NH_3 to NO_2^- *via* a homogeneous

electrocatalytic process mediated by redox transformations of $Cu(OH)^{4-/2-}$ species in solutions that dissolve from the electrode. The second pathway is the heterogeneous electrocatalytic oxidation of NH_3 on the electrode surface favoring the formation of NO_3^-. By virtue of its nature, the homogeneous mediated pathway enables higher selectivity and is less affected by electrode poisoning with the strongly adsorbed "N" intermediates that has plagued the electrocatalytic ammonia oxidation field. Thus, the selectivity of the Cu-catalyzed NH_3 oxidation towards either nitrite or nitrate can be achieved through balancing the kinetics of the two mechanisms by adjusting the pH of the electrolyte medium and potential.

Introduction

The electrocatalytic oxidation of ammonia has been studied in detail due to its inherent utility in a number of applications such as fuel cells,[1–4] for the remediation of wastewater systems,[5–9] for sensors,[10–12] and for bulk electrolysis in systems where ammonia acts as a hydrogen carrier.[13] The major and most desired product in these processes is N_2, while the formation of the oxidized compounds of nitrogen is usually considered highly undesirable. On the other hand, driving the catalytic oxidation towards the formation of nitrites and nitrates might open up the possibility of a low-temperature electrochemical processes for small to medium scale, renewable-powered production of these important commodity chemicals. Currently, the bulk of the research conducted on the ammonia oxidation reaction (AOR) has been focused on the use of noble metal-based catalysts such as platinum, palladium, rhodium and iridium.[14–16] Among these, platinum is the most widely studied with literature dating back more than a century.[17]

The platinum-catalyzed AOR is a complex, multistep heterogenous reaction which was in particular scrutinized by Gerischer and Mauerer in 1970.[18] Overall, the reaction is known to be sluggish and poorly selective with a variety of nitrogenous products being generated. Another notable issue of noble metal based systems is their tendency to become poisoned by strongly adsorbed N_{ads} species during the oxidation process.[19] At very positive potentials, the platinum surface is further poisoned by adsorbed NO_x products, resulting in the rapid deterioration of the catalyst's performance.[14] This, combined with the inherent scalability issues that come with the use of expensive noble metal catalysts, makes platinum-based AOR an unlikely prospect for commercialization. To address these issues, investigations have begun into the possibility of the AOR catalysis by the electrodes based on earth-abundant first-row transition metals. Some initial studies into the AOR catalyzed by such metals have shown that nickel exhibits a reasonable

activity.[20–22] While this is clearly a step in the right direction, the selectivity provided by this material is poor, with a variety of products formed, namely NO_2^-, NO_3^- and N_2.[22]

In nature, ammonia oxidation is promoted by the ammonium monooxygenase enzyme, which is a naturally occurring AOR catalyst with a copper(II)-based catalytically active centre.[23,24] A theoretical mechanistic study by Herron *et al*. also identified copper (along with iridium) as a prime candidate for the catalysis of the electrochemical oxidation of ammonia, second only to platinum.[25] A more recent experimental study focused on a mixture of nickel oxyhydroxides and copper hydroxides has shown that copper in the form of copper(II) hydroxide exhibits catalytic activity for the AOR.[26] Most notably, the primary oxidation product of the $Cu(OH)_2$-catalyzed process is NO_2^-. This study also suggested that the AOR on copper, nickel and mixed hydroxides mostly occurs *via* a classical heterogeneous electrocatalytic mechanism, with intermediate adsorbates such as $*NH_2$ and *NO detected on the surface by *in situ* FTIR spectroscopy.[26] However, despite its proven activity[26] and theoretical predictions,[25] copper has been largely overlooked as an AOR catalyst. This is in part due to the fact that copper is prone to electrodissolution by ammonia under alkaline conditions. In a study by de Vooys *et al*. on the role of adsorbates during the AOR, it was concluded that Cu electrodissolution took place with 100% faradaic efficiency at pH 14 with a predominant formation of the copper complex with ammonia.[19] As such, materials based on this metal would seem to be a poor choice for an AOR catalyst. However, as we demonstrate in this study, the issues of Cu dissolution and complexation of copper cations with ammonia can be mitigated to a reasonable extent by fine-tuning both the pH and operating conditions, and these may in fact be the key to achieving a highly selective electrocatalytic ammonia oxidation to either nitrite or nitrate.

Experimental

Materials. Electrolyte solutions consisted of KOH (*Merck*; ≥ 85%, acidimetric) and NH_4OH solution (*Sigma-Aldrich*; 99.99%) dissolved in H_2O derived from the *Satorius™ Arium® Comfort II* water purification system (measured resistivity 18.2 MΩ cm at ambient temperature; 24 ± 1 °C). Solutions were prepared in three electrolyte concentrations: 0.011, 0.11 and 1.1 M KOH for background electrode characterizations and the same with the addition of 0.10 M NH_4OH for the electrocatalytic tests. The concentration of the 1.1 M KOH solution was determined *via* titration, while the 0.11 and 0.011 M solutions were made *via* dilution of the 1.1 and 0.11 M solutions, respectively. Electropolished Cu plate working electrodes (99.98% pure copper supplied by *Sigma-Aldrich*) were used for cyclic voltammetric studies only, while electropolished copper wire (99.8% pure supplied by *Thermofisher Scientific*) was used for chronoamperometric experiments. These were in some cases preceded and followed by voltammetric analysis to confirm that the electrochemical behavior was reproducible. Copper electrodes were newly constructed and electropolished for each experiment to ensure that all electrodes had homogeneous surfaces, and to minimize the discrepancy between geometric and real surface area during measurements. Electropolishing of the copper electrodes was conducted in solutions that consisted of 85 % orthophosphoric acid purchased from *Chem-supply Pty Ltd*, and 0.1% w/v of soluble starch supplied by *Ajax Finechem*.

Electrochemical experiments. All measurements were conducted using a *Gamry Instruments Interface 1000 E* potentiostat operated in a three-electrode configuration, except for the electropolishing experiments which were undertaken in a two-electrode mode. The latter procedure was applied to all copper working electrodes investigated herein, using the electrolyte solution identified above and a high-surface area copper wire counter electrode at an applied potential of 4.7 V for 4 min for newly constructed plate electrodes (further details on this procedure

are provided in Figures S1-S2 and in the "Electro-polishing of copper electrodes" section of the Supporting Information).

As both alkaline media and ammonia are well-known to damage standard Ag|AgCl electrodes, custom reference systems were built for each pH range, depending on the intended use. Details regarding design and construction are included in Figures S3-S5 and in the 'Custom Reference Electrodes' section of the Supporting Information. All the references designed for this study were based around the $Cu^{1+/2+}$ redox couple and had a stable potential around 0.24 V *vs*. standard hydrogen electrode (SHE). Unless otherwise stated, all potentials listed here are quoted relative to the reversible hydrogen electrode (RHE) scale, which were calculated using the Nernst equation. pH values of 12.0, 12.9 and 13.9 for the electrolyte solutions containing 0.011, 0.11 and 1.10 KOH respectively, were used based on the experimentally determined KOH concentrations.[27]

Measurements were conducted in a set of 15 mL test tubes (Figure S6). Rubber septa supplied by *Sigma-Aldrich* were used to achieve air tightness where necessary. For measurements under continuous argon gas purge, a saturator containing the working electrolyte was used to maintain the concentration of ammonia throughout the duration of the experiment. In addition, a water lock was employed for gas flow out of the headspace to prevent backflow of oxygen into the electrolytic cell. A platinum wire coil separated from the primary working electrode compartment by a P4 ceramic frit served as the auxiliary electrode.

***In situ* Raman spectroscopy.** Raman spectra were obtained using a *Renishaw Invia* microscope with 63 nm excitation delivering 1.5 mW at the sample. Spectra were acquired in static mode over a range of 100 to 988 cm^{-1} with exposure duration of 4 seconds and 20 co-added scans. An *Olympus 50X* long working distance lens (*ca* 8 mm) was employed to focus on the exposed solution at the surface of the electrode. *Renishaw WiRE 3.4* software controlled the microscope

and data processing. These measurements were performed using a custom-made cell, the details of which are included in the '*In situ* Raman spectroscopy' section of the Supporting Information.

Quantitative analysis of nitrite and nitrate. Dissolved reaction products were quantitatively analyzed using ion chromatography on a *DIONEX Integrion HPIC ThermoFisher Scientific* instrument. Each individual scan had a total elution time of 10 minutes and employed KOH as the eluent compound and an eluent flow rate of 0.380 mL min^{-1}. Eluent concentration was varied throughout the measurement in a two-stage gradient. In stage one, the gradient was elevated linearly from 0.001 M KOH at $t = 0$ to 0.050 M at $t = 5$ min (ramping rate 0.010 M min^{-1}). In stage two, an inverse gradient was employed, with the concentration declining from 0.050 M KOH at $t = 5$ min down to 0.001 M at $t = 10$ min (ramping rate -0.010 M min^{-1}). The column, conductivity suppressor and conductivity detection cell were maintained at a temperature of 30 °C during the measurements. The standard addition method was used for peak identification and quantification of target products NO_2^- and NO_3^-. A total of 6 additions with concentrations of 6.25, 12.5, 25, 50, 100 and 200 μM of both NO_2^- and NO_3^- were done for each sample of the electrolyte solution for a total of 7 separate 10-minute runs (6 spiked samples and 1 un-spiked sample of equal dilution). Further details on the specific methodology used are included in the "Ion Chromatography" section in the Supporting Information.

Faradaic efficiency of the AOR with respect to NO_2^- and NO_3^- was calculated as nFN_{NOx} / Q, where the number of electrons $n = 6$ and 8, respectively, $F = 96485.3$ C mol^{-1} is the Faraday's constant, N_{NOx} / mol is the amount of the product formed, and Q / C is the total charge passed during the measurement.

Scanning electron microscopy (SEM) was used to assess the effectiveness of the electropolishing method developed during this work (see "Electropolishing of copper electrodes" section of the Supporting Information). Micrographs were collected using a *FEI Nova NanoSEM 450* instrument on the electrodes immobilized on the SEM stubs using a conductive sticky tape.

Inductively Coupled Plasma – Optical Emission Spectrometric (ICP-OES) analysis of the electrolyte solutions kept in contact with Cu electrodes without and with potential applied was undertaken using a *PerkinElmer Avio 200* instrument. Copper standards were prepared *via* dilution of a gravimetrically prepared stock of copper sulphate (99 – 105% purchased from *EMSURE*®) to produce a calibration curve within a concentration range from 0.01 to 100 μM. All electrolyte samples and copper standards were diluted with aqueous 2 vol.% HNO_3, which was also used as an eluent solution. As the variance in both the axially and radially acquired data was approximately equal across all measurements, the values presented are the average of both.

Results and Discussion

This investigation commenced with cyclic voltammetry to identify the effects of pH and addition of ammonium hydroxide to the solution. Following this, *in situ* Raman spectroscopy was used to probe the catalytically active state of copper at the potentials where the AOR occurs and observe changes with the addition of ammonium hydroxide to corroborate the voltammetric findings. A series of long-term electrocatalytic and control experiments was then carried out to understand the product distribution as a function of the applied potential and pH.

Cyclic voltammetry

After electropolishing, cyclic voltammograms of both copper plate and wire electrodes exhibited a pattern of signals typical of polycrystalline Cu, which are best observed at the highest KOH

electrolyte concentration examined herein, *viz.* 1.1 M (Figure 1A). Specifically, there are four primary oxidation peaks in the anodic sweeps, as well as four reduction processes in the cathodic sweeps. Peak A1 at *ca* 0.51 V (all potentials herein are referenced to the reversible hydrogen electrode, RHE) is associated with the oxidation of Cu^0 to Cu^+, primarily with the formation of Cu_2O.[28] Processes A2 and A3 both generate a mixture of products: the former includes the oxidation of metallic Cu to both Cu_2O and soluble Cu^{2+} species such as $Cu^{II}(OH)_4^{2-}$,[28] while the latter represents the conversion of copper metal into $Cu(OH)_2$ and CuO depending on conditions.[28,29] Lastly, peak A4 is associated with the formation of various Cu^{3+} compounds, such as the soluble $Cu^{III}(OH)_4^-$ species as well as surface layers of Cu_2O_3 and CuOOH.[28,30–32] On the reverse sweep, Cu^{3+} compounds are reduced to Cu^{2+} (peak C4), followed by its further reduction to Cu^+ (peak C3) and finally the reduction of the remaining Cu^+ and Cu^{2+} species to Cu^0 (peaks C2 and C1, respectively).[28,29,33] Note that the numbering of the voltammetric peaks in Figure 1A-C does not reflect coupling between particular anodic and cathodic processes due to their different electrochemical nature in most cases, with the exception of a reasonably well-defined $Cu^{2+/3+}$ (A4/C4) redox couple.

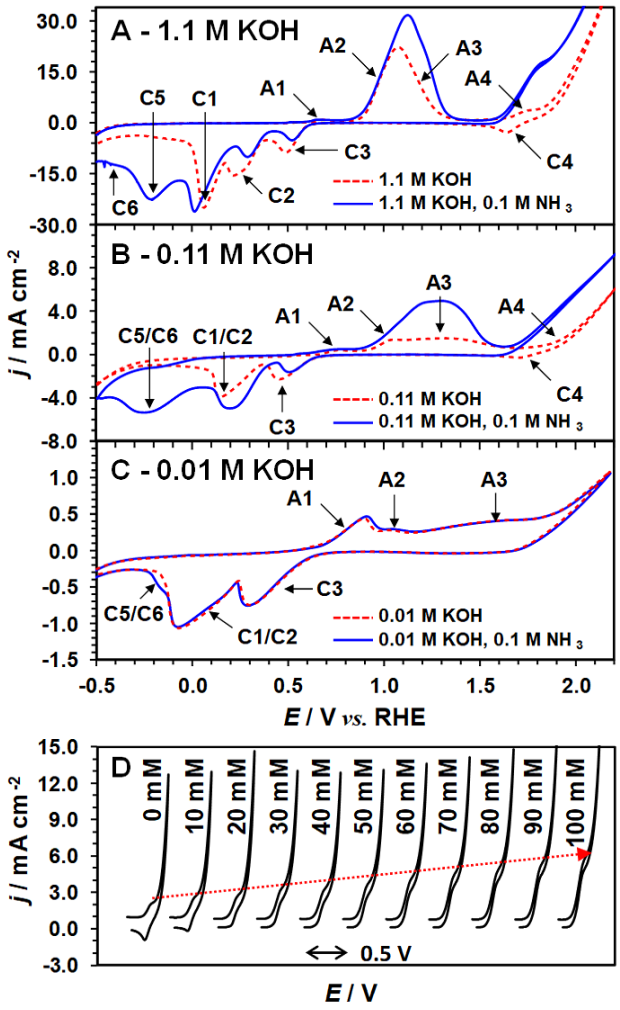

Figure 1. Comparison of cyclic voltammograms (scan rate 0.100 V s^{-1}) of a Cu electrode recorded in (A) 0.011, (B) 0.11 and (C) 1.1 M KOH in the absence (*dashed red*) and presence (*solid blue*) of 0.10 M NH_3. (D) Stacked cyclic voltammetry focused on the $Cu^{2+/3+}$ redox couple (1.4-1.8 V *vs.* RHE range; 0.100 V s^{-1}) in 1.1 M KOH with increasing concentrations of NH_3. Note different ordinate scale ranges in all panels. Currents are normalized to the geometric surface of the electrodes.

In 0.11 M KOH, the intensity of all major redox peaks is substantially suppressed and peaks A4 and C4 are poorly defined as compared to the data recorded in 1.1 M KOH (*cf.* Figure 1A and 1B). The latter observation is consistent with the more favorable formation of CuO and suppressed

corrosion of the electrode to generate soluble $Cu^{II}(OH)_4^{2-}$ and $Cu^{III}(OH)_4^-$. In the least alkaline solution investigated in the present study (0.011 M KOH), the voltammetric pattern is qualitatively similar to that in 0.11 M KOH, and the solubility of copper is even further lowered.[34] As such, the $Cu^{2+/3+}$ redox peaks (processes A4/C4 shown in Figure 1A and 1B) are practically not observable in Figure 1C as they are dependent on the preceding dissolution reaction.

The introduction of NH_3 into the system resulted in several important changes in the cyclic voltammetric profiles (Figure 1A-C). There is an enhancement in the magnitude of the process A2 that generates soluble Cu^{2+} species across all KOH concentrations examined. The same feature was seen by de Vooys *et al*. and was attributed to the formation of copper ion-ammonia complexes.[19] This complex formation can be seen most clearly in 0.11 M KOH with the enhancement of the oxidation peak at *ca* 1.05 V. In 1.1 M KOH, two new reduction peaks appear at *ca* -0.20 and -0.40 V (processes C5 and C6 in Figure 1A) just prior to the onset of the hydrogen reduction reaction at approximately -0.50 V. These signals might be associated with the reduction of the NH_3 oxidation products, primarily NO_2^- and NO_3^-, as described by Davis *et al*.[35] and confirmed by control experiments undertaken herein (Figure S19). In 0.11 M KOH, these peaks appear to merge into a single broad peak with the maximum at *ca* -0.25 V, while in 0.011 M KOH this signal is merged with peak C1/C2 to form a small shoulder at *ca* -0.20 V.

Perhaps the most significant change in the voltammetry in the presence of NH_3 is associated with the $Cu^{2+/3+}$ redox processes (peak A4) in 1.1 M KOH (Figure 1A). There is a clear enhancement to the oxidation current of this process, with a more than three-fold increase in the peak current density relative to the data obtained in the absence of ammonia. Conversely, the corresponding Cu^{3+} reduction peak is completely absent. Both observations suggest that the Cu^{3+} ions generated during the anodic sweep are being rapidly consumed by the process of ammonia

oxidation, wherein Cu^{3+} acts as a strong chemical oxidant. This results in the regeneration of Cu^{2+}, which can be electrochemically re-oxidized at the electrode forming a classical homogeneous electrocatalytic (redox mediated) process.[36,37] This then leaves a negligible quantity of Cu^{3+} remaining to be reduced in the cathodic sweep, hence the absence of the corresponding reduction peak. The possibility that Cu^{3+} is being reduced to an oxidation state lower than 2+ in its reaction with ammonia was considered. However, the lack of significant changes in the reductive charge recorded during backward voltammetric sweeps (Figure 1A) does not support this hypothesis. Indeed, if Cu^{3+} was being reduced by ammonia to Cu^{+} or Cu^{0} at a significant rate, the magnitude of the other cathodic peaks (C1-C3) would diminish and this effect would be best seen in process C3 ($Cu^{2+/1+}$), in which the total charge is similar to that for C4 ($Cu^{3+/2+}$). The Cu^{3+} mediated ammonia oxidation can also be verified by the close-to-linear relationship between the A4 peak current densities and ammonia concentration (Figure 1D). As expected, the $Cu^{2+/3+}$ oxidative peak increases in magnitude with the ammonia concentration and a concomitant suppression of the reductive peak C4, which drops to zero at an ammonia concentration of 40 mM, is observed. With more NH_3 added to the solution, the A4 peak progressively takes on the appearance of an S-shaped signal. While this is typically indicative of a kinetically limited process,[36] interference from the water oxidation process makes further kinetic analysis impractical.

The voltammetric evidence of the electrocatalytic ammonia oxidation in 0.11 and 0.011 M KOH is less obvious than in 1.1 M KOH. In regards to 0.11 M KOH (Figure 1B), the changes in the voltammetry occurring at potentials more negative than 1.7 V are not associated with the catalytic oxidation of ammonia, but rather the enhancement of electrodissolution of Cu^{2+} species.[19] At potentials more positive than 1.7 V, peak C4 is reduced in magnitude relative to scans conducted in 1.1 M KOH due to the reduced solubility of copper in 0.11 M KOH. This effect is even more

pronounced with peak A4, as it is effectively indistinguishable from the oxygen evolution reaction (OER) signal in the absence of ammonia. However, when ammonia is present, there is a clear enhancement of the oxidative current relative to the blank scan and peak C4 vanishes entirely, as was the case in 1.1 M KOH, indicating that the catalytic oxidation of ammonia is taking place. Also, of note is the appearance of the aforementioned reduction peak at *ca* -0.25 V (processes C5/C6). In 0.011 M KOH, there is little to indicate that the oxidation of ammonia is taking place. The sole indicator of ammonia oxidation is the appearance of the cathodic shoulder at *ca* -0.20 V.

In-situ Raman spectroscopy: identification of copper (III)

The formation of the Cu^{3+} species upon electrooxidation of the copper electrodes can be confirmed by Raman spectroscopic analysis undertaken *in situ*.[32] Herein, this was done using specifically designed spectroelectrochemical cells (see "*In situ* Raman spectroscopy" in the Supporting Information) to monitor the surface changes that occur at a range of applied potentials in the absence and in the presence of ammonia in 0.11 M KOH. For improved clarity, the data presented in Figure 2B have been smoothed, while the unsmoothed data are available in the Supporting Information (Figure S9). The potentials used in these experiments were expected to favor the formation of Cu^{0} (*ca* -0.3 V), Cu^{1+} (*ca* 0.6 V), Cu^{2+} (*ca* 1.2 V) and Cu^{3+} (*ca* 1.7 V) compounds, as indicated by the colored markers on the Pourbaix diagram shown in Figure 2A. *In situ* Raman data for Cu electrodes in alkaline electrolyte solutions at other potentials within a 0.78-1.62 V range can be found in a publication by Deng *et al.*[32] Herein, scans at *ca* -0.3 V produced featureless curves, as would be expected for copper metal (Figure 2B). The Raman spectra collected at both 0.6 V and 1.2 V (Cu^{1+} and Cu^{2+}) showed two sets of broad peaks, the first ranging from 460 to 540 cm^{-1} and the second ranging from 560 to 630 cm^{-1}. This indicates that in both cases the surface

is dominated by copper hydroxides, as concluded from the comparisons of this data to the previously published results (see the $Cu(OH)_2$ reference data in Figure 2B).[32]

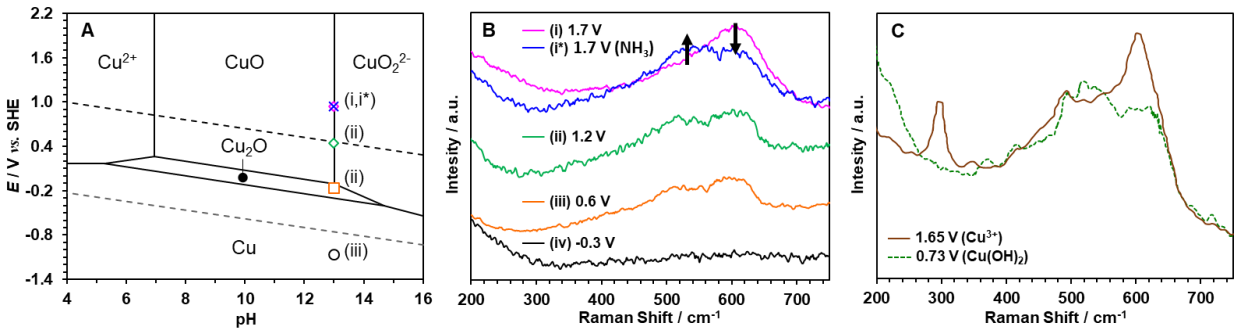

Figure 2. (A) Pourbaix diagram of copper (10 µM Cu^+, 25 °C) digitized and reproduced from Ref.[34] (note that Cu^{III} species are not included in the calculation of the diagram as these are either not the thermodynamically stable species or data is not available for them). Markers indicate corresponding potentials at pH = 13 used for *in situ* Raman experiments shown in panel B. (B) *In situ* Raman spectroelectrochemical analysis of a copper electrode in contact with quiescent 0.11 M KOH at -0.3 (*black*), 0.6 (*orange*), 1.2 (*green*) and 1.7 V *vs.* RHE (*magenta*) and in 0.10 M NH_3 + 0.11 M KOH at 1.7 V *vs.* RHE (*blue*); arrows highlight the changes in spectra induced by the presence of ammonia. (C) Previously reported spectra for $Cu(OH)_2$ in 0.10 M KOH at 0.73 (*green dashed*) and 1.65 V *vs.* RHE (*brown solid*); digitized from Ref.[32]

Most interestingly, an increase of the positive potential beyond the point of Cu^{3+} formation (1.7 V) induced a decrease in the relative intensity at *ca* 500 cm^{-1} and clearly produced a new peak at *ca* 600 cm^{-1} (Figure 2B). The latter signal was reported to correspond to Cu^{3+} oxide species (Figure 2C),[32] thus confirming its existence at the surface of the copper electrodes at potentials where significant rates of the ammonia oxidation are observed (Figure 1B). The shape of the Raman spectra recorded at 1.7 V also suggests that the surface contains a mixture of the Cu^{2+} and Cu^{3+} states. Of equal importance, addition of 0.10 M ammonia to the electrolyte solution,

suppressed the Raman peak corresponding to Cu^{3+} (Figure 2B), which is concordant with the mediated mechanism described above. In other words, NH_3 rapidly reacts with any electrochemically generated Cu^{3+} species with the formation of Cu^{2+} hydroxides, which dominate the Raman signal even at the very positive potential of 1.7 V when ammonia is present (Figure 2B).

Chronoamperometry: oxidation products and stability

Chronoamperometric experiments were undertaken to investigate the stability of a copper electrocatalyst in operation and identify the effects of potential on the products of ammonia oxidation. As hypothesized above, based on the analysis of voltammetric data, the production of nitrite and nitrate was found to be insignificant at potentials more negative than 1.7 V (Figures S17 and S18). Hence, all further analysis focused on the potential range of 1.7-2.0 V. Under these conditions, the magnitude of the anodic current densities was similar at all KOH concentrations examined herein (Figure 3A-C). However, there were marked differences in the NO_2^-/NO_3^- yield rates and the faradaic efficiencies resulting from the chronoamperometric experiments. Part of the difference seen here is the loss of the faradaic efficiency due to water oxidation. In 0.011 M KOH, gas bubbles formed on the electrode surface throughout the course of experiments at 1.8, 1.9 and 2.0 V. This produced large fluctuations in current density as gas bubbles were released from the electrode surface (Figure 3A). As such, the faradaic efficiency in experiments conducted in 0.011 M KOH between 1.8 and 2.0 V was diminished (Figure 3E). However, there was no sign of gas evolution at the KOH concentrations of 0.11 and 1.1 M.

Another key factor driving the variations in the NO_2^-/NO_3^- faradaic efficiency and yield rate is the difference in the solubility of copper at each of the KOH concentrations tested herein. As pH is lowered, the solubility of copper declines, reaching a minima at pH 10.[38] As such, the highest

possible concentration of dissolved copper species in solution is significantly lower in 0.011 M KOH than it is in 0.11 and 1.1 M KOH. This was confirmed through the ICP-OES analysis of the electrolyte solutions of interest in contact with Cu electrodes to monitor the concentration of dissolved copper over time (Table S2). These effects manifest in the roughening of the electrocatalyst as anodized copper is dissolved, followed by the formation of $Cu(OH)_2$ at the electrode surface once the solution becomes saturated (see Figure S8 in Supporting Information for image and Raman data). In 0.011 M KOH, this can be seen at 1.8, 1.9 and 2.0 V, where the current rises for the first 10 to 20 min while the electrocatalyst is roughened, and begins to decline as the solution reaches saturation and a layer of $Cu(OH)_2$ begins to form (Figure 3A). In 0.11 M KOH, a higher amount of copper species can be dissolved than at lower pH. As a result, the saturation of the solution with these species was not reached within the duration of the experiment, resulting in the steady increase in the oxidative current density as the electrode became roughened (Figure 3B). Although the most significant dissolution occurs in 1.1 M KOH, the electroactive surface area did not appear to be significantly enhanced under these conditions resulting in relatively constant current densities (Figure 3C).

Apart from the products of water and copper electrooxidation, additional side products that can be formed include N_2,[39] as well as other intermediate species of the ammonia oxidation including hydroxylamine.[40] Taken together, the formation of these side products does not allow for achieving 100% faradaic efficiency of the ammonia oxidation reaction with respect to nitrite and nitrate – the target products of the present work.

Marked differences were also seen in the NO_2^- and NO_3^- product yields at various pH and applied potentials (Figure 3D). The product yield rates show a progressive increase in the proportion of NO_3^- generated at increasingly positive potentials, with essentially no NO_3^- detected at any pH at

1.7 V, but with the notable amount produced at all other potentials examined. In a different trend, as the pH of the electrolytes was increased, the proportion of NO_3^- decreased with respect to the total NO_2^- + NO_3^- yield. For example, the percentage of NO_3^- of the total NO_x produced at 1.9 V was *ca* 85%, 43% and 14% in 0.011, 0.11 and 1.1 M KOH, respectively.

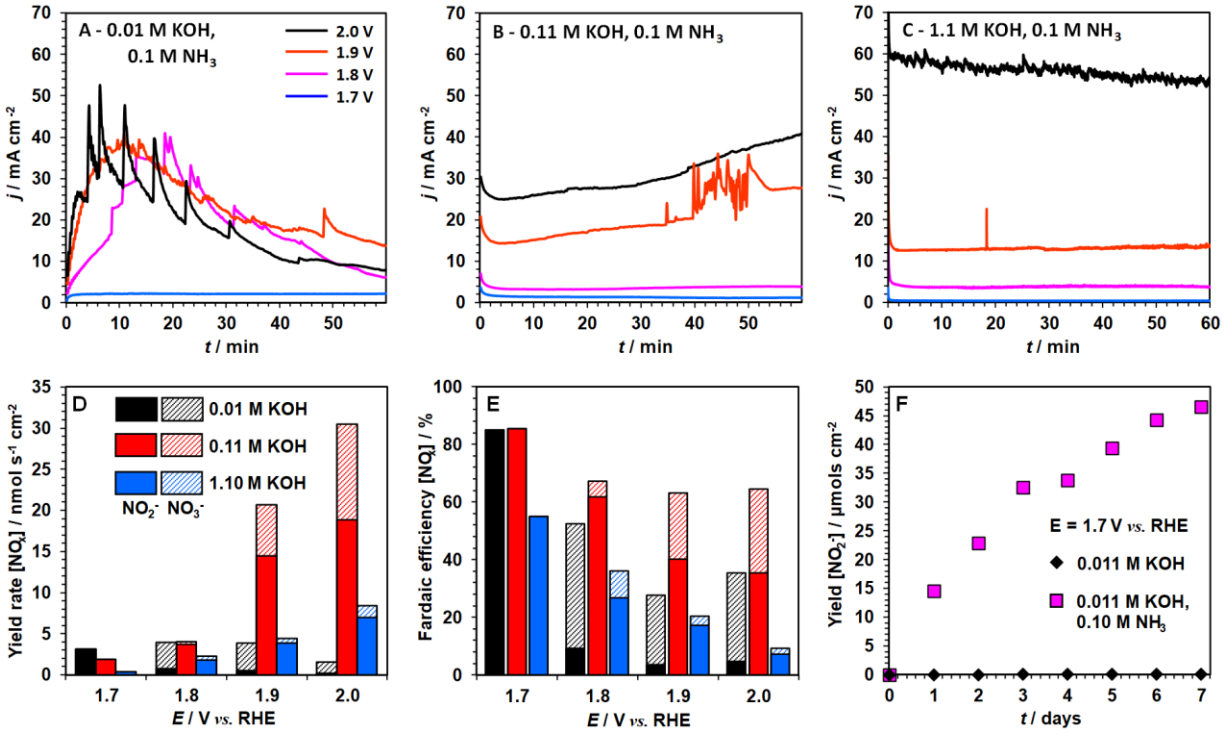

Figure 3. Potentiostatic oxidation of 0.10 M NH_3 with a copper electrode at different KOH electrolyte concentrations. (A-C) Chronoamperograms collected at indicated potentials (V *vs.* RHE) in the presence of 0.011, 0.11 and 1.1 M KOH. (D) Comparative yield rate data for nitrite (*solid*) and nitrate (*hashed*), and (E) comparative faradaic efficiency data for nitrite (*solid*) and nitrate (*hashed*) in 0.011 (*black*), 0.11 (*red*) and 1.1 M KOH (*blue*) as a function of potential. (F) Cumulative yield of NO_2^- during a 7-day chronoamperometric experiment at 1.7 V vs. RHE in 0.011 M KOH with (*magenta*) and without (*black*) 0.1 M NH_3 added.

In terms of the overall AOR catalytic performance, the highest faradaic efficiency for the conversion of NH_3 to NO_2^- and NO_3^- on copper is observed in 0.11 M KOH at 1.7 V (Figure 3E).

Under these conditions, approximately 90% of current is associated with the formation of NO_2^-. At the same KOH concentration, but at 2.0 V, the overall faradaic efficiency declines to 65%, though now with a 36% contribution from the NH_3 to NO_2^- reaction and a 29% contribution from the NH_3 to NO_3^- reaction. This same general decline in the faradaic efficiency towards NO_2^- + NO_3^- with positively increasing potential was seen at every KOH concentration examined. This is most likely due to the increased contribution from the copper-catalyzed OER.[41] This was particularly true in 0.011 M KOH where oxygen formation was visibly apparent and dominant, as discussed above. In contrast, the nitrite and nitrate yield rates significantly increased at 1.9-2.0 V in 0.11 M KOH, with the best result of 30 nmol s^{-1} cm^{-2}, 38% of which was NO_3^-, obtained at the most positive potential examined herein (Figure 2B). However, with higher KOH concentration of 1.1 M there is an overall drop in both the yield rate and faradaic efficiency (Figure 3D-E). This can be attributed to the domination of the copper electrodissolution reaction over both the AOR and OER reactions, as reported by de Vooys *et al.*[20] and confirmed by the observation of the transition of the electrolyte hue to a bluish solution herein.

Mechanism of the Cu-catalyzed ammonia electrooxidation

Based on the data collected in the present study, it is hypothesized that the electrooxidation of NH_3 over copper catalysts results from a pH and potential-dependent interplay of two major mechanisms: (A) a homogeneous electrocatalytic $Cu^{2+/3+}$ mediated process, and (B) heterogeneous electrocatalytic reaction occurring through the adsorption and further surface-confined transformations of NH_3 on the catalyst surface (Figure 4). Furthermore, based on the reasoning presented below we suggest that pathway (A) favors the formation of NO_2^-, while nitrate is the preferred product of mechanism (B).

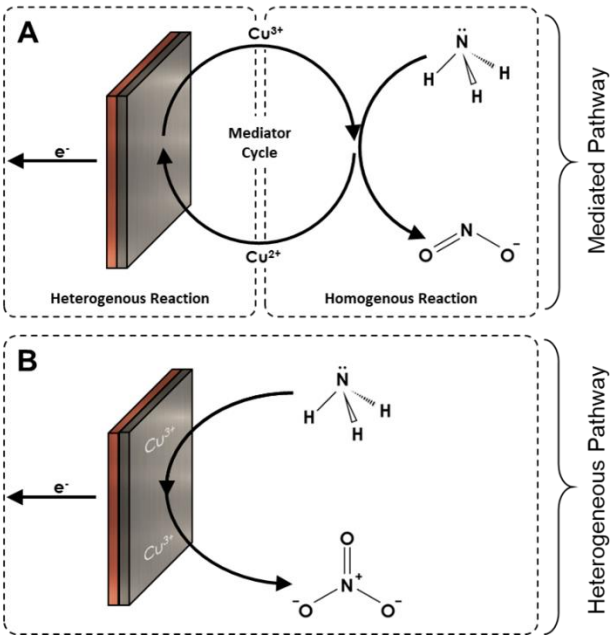

Figure 4. Diagram illustrating the two proposed pathways for the copper-catalyzed AOR: (A) homogeneous electrocatalytic (mediated) oxidation where the primary product is NO_2^-, and (B) direct heterogenous electrocatalytic oxidation of NH_3 where the primary product is NO_3^-.

The Pourbaix diagram of copper indicates that change in pH from values below 13 to more alkaline environment (at potentials more positive than -0.1 V *vs.* SHE, as is always the case in the analysis herein) alters the thermodynamically preferred state from solid $Cu^{II}O$ to dissolved copper(II) species (Figure 2A). This means that the formation of $Cu^{II}(OH)_4^{2-}$, which is further oxidized in process A4 and thereby catalyzes the electrooxidation of NH_3 (Figure 1A), strongly depends on pH. Based on this and the analysis of the voltammetric data, it would be expected that the $Cu^{2+/3+}$ species would form in trace amounts in 0.011 M KOH, small to moderate concentrations in 0.11 M KOH, and relatively large concentrations in 1.1 M KOH. Based on this, it follows that the NH_3 oxidation through a homogeneous electrocatalytic mechanism mediated by the $Cu^{2+/3+}$ redox couple has the lowest contributions in 0.011 M KOH. Notably, the proportion of produced NO_2^- is very low in 0.011 M KOH (except at 1.7 V, which is discussed separately below),

and the largest in 1.1 M KOH where, by comparison a minimal amount of nitrate is produced (Figure 3D). Therefore, it can be proposed that the primary product of the homogeneous $Cu^{2+/3+}$ mediated ammonia oxidation is nitrite.

Given the fact that the homogeneous electrocatalytic mechanism is not clearly detected in 0.011 M KOH by voltammetry and nitrate is predominantly produced under these conditions (except for tests at 1.7 V), it is further suggested that the heterogeneous catalytic pathway is primarily responsible for the NH_3 oxidation at this pH but requires positive potentials of at least 1.8 V. At 1.7 V in 0.011 M KOH, small concentrations of dissolved $Cu^{2+/3+}$ species still exist (Table S2) and are capable of maintaining the homogeneous NH_3 oxidation to NO_2^-. In 0.11 M KOH, both processes compete with each other depending on the applied potential: more negative than 1.9 V, catalytic oxidation mediated by electrogenerated dissolved Cu^{3+} dominates, which is further accelerated at 1.9 and 2.0 V yet with an increased contribution of the heterogenous reaction (3D and 3E).

While the heterogenous catalytic mechanism is directly converting ammonia to NO_3^-, which may be considered desirable for certain applications, *i.e.* nitric acid and fertilizer production, it is in direct competition with the OER reaction and is therefore not highly selective. In addition, being a heterogenous electrocatalytic process, the possibility of electrode degradation or poisoning effects is still a concern. Conversely, the homogeneous electrocatalytic pathway has some attractive features, namely improved selectivity towards a single product (NO_2^-) and an intrinsic resistance to electrode poisoning. Indeed, as ammonia is not reacting on the electrode surface, the formation of poisoning adsorbates should be effectively negated. To demonstrate this, long-term chronoamperometric experiments were run over a period of one week in 0.011 M KOH and at a potential of 1.7 V in an attempt to isolate the mediated homogeneous catalytic reaction from the

direct heterogeneous mechanism and to minimize electrode dissolution. Control experiments undertaken either in the absence of ammonia (Figure 3F and Figure S20a) or with no potential applied (Figure S20b) show negligible amounts of nitrite and nitrate accumulated, most probably as a contamination entering the electrolyte solution during sampling. In contrast, the cumulative yield of NO_2^- in the actual AOR experiment progressively increased over one week of testing (Figure 3F) while the concentration of dissolved copper remained constant (Table S2). Taken together, these results support our hypothesis that no significant electrode poisoning occurs when the homogeneous electrocatalytic process is the dominant reaction pathway. If this mode of operation could be further optimized to produce the fully oxidized NO_3^- product, it may prove to be a highly selective and robust method of electrocatalytic ammonia oxidation.

Conclusions

In this work we have demonstrated that the catalytic ammonia electrooxidation on copper electrodes follows two main pathways: a heterogeneous pathway of which the primary product is NO_3^-, and a homogeneous mediated reaction pathway where the primary product is NO_2^-. The mediator species was $Cu(OH)_4^-$ in which the copper cycles between the 2+ and 3+ oxidation states. Potentiostatic electrocatalytic experiments showed that the best overall yield was obtained at 2.0 V *vs*. RHE in 0.11 M KOH with a faradaic efficiency of 65% with a total NO_2^-+NO_3^- yield rate of 30 nmols s^{-1} cm^{-2}. Products in this case were 38% NO_3^- and 62% NO_2^-, indicating that the homogeneous electrocatalytic mechanism is more preferred. While both reaction pathways present advantages, the homogeneous mechanism offers superior selectivity and has an innate resistance to the effects of electrode poisoning due to the AOR occurring in the solution phase. This was demonstrated through long-term catalytic tests enabling steady conversion of ammonia to nitrite.

As such copper-mediated ammonia oxidation may provide a foundation for the development of selective AOR catalysts.

Acknowledgements

The authors thank Monash Centre for Electron Microscopy (MCEM) for the provision of access to their instruments, Mr. Finlay Shanks for his training and assistance with Raman spectroscopy, Dr Jacinta Bakker for the assistance with setting up the IC analysis, and Dr Federico F. Vallana for his assistance with ICP-OES experiments. This study was supported by the Australian Research Council through the Australian Centre for Electromaterials Science (CE140100012), Discovery Project (DP200101491), DRM's Australian Laureate Fellowship (FL120100019), ANS's Future Fellowship (FT200100317), Monash-Warwick joint PhD program (to BT) and the University of Southampton Research Placement Program (LK).

Conflicts of Interest

The authors declare no conflicts of interest.

References

(1) Cairns, E. J.; Simons, E. L.; Tevebaugh, A. D. Ammonia-Oxygen Fuel Cell. *Nature* **1968**, *217* (5130), 780–781. https://doi.org/10.1038/217780a0.

(2) Simons, E. L.; Surd, D. J.; Cairns, E. J. Performance of Direct Ammonia Fuel Cells. *J. Electrochem. Soc.* **1969**, *116* (5), 131–138.

(3) Suzuki, S.; Muroyama, H.; Matsui, T.; Eguchi, K. Fundamental Studies on Direct Ammonia Fuel Cell Employing Anion Exchange Membrane. *J. Power Sources* **2012**, *208*, 257–262. https://doi.org/10.1016/j.jpowsour.2012.02.043.

(4) Assumpção, M. H. M. T.; Da Silva, S. G.; De Souza, R. F. B.; Buzzo, G. S.; Spinacé, E. V.; Neto, A. O.; Silva, J. C. M. Direct Ammonia Fuel Cell Performance Using PtIr/C as Anode Electrocatalysts. *Int. J. Hydrogen Energy* **2014**, *39* (10), 5148–5152. https://doi.org/10.1016/j.ijhydene.2014.01.053.

(5) Marinčić, L.; Leitz, F. B. Electro-Oxidation of Ammonia in Waste Water. *J. Appl. Electrochem.* **1978**, *8* (4), 333–345. https://doi.org/10.1007/BF00612687.

(6) Bonnin, E. P.; Biddinger, E. J.; Botte, G. G. Effect of Catalyst on Electrolysis of Ammonia Effluents. *J. Power Sources* **2008**, *182* (1), 284–290. https://doi.org/10.1016/j.jpowsour.2008.03.046.

(7) Li, L.; Liu, Y. Ammonia Removal in Electrochemical Oxidation: Mechanism and Pseudo-Kinetics. *J. Hazard. Mater.* **2009**, *161* (2–3), 1010–1016. https://doi.org/10.1016/j.jhazmat.2008.04.047.

(8) Zöllig, H.; Fritzsche, C.; Morgenroth, E.; Udert, K. M. Direct Electrochemical Oxidation of Ammonia on Graphite as a Treatment Option for Stored Source-Separated Urine. *Water Res.* **2015**, *69*, 284–294. https://doi.org/10.1016/j.watres.2014.11.031.

(9) Diaz, L. A.; Botte, G. G. Hydrodynamic Analysis and Simulation of a Flow Cell Ammonia Electrolyzer. *Electrochim. Acta* **2015**, *179*, 529–537. https://doi.org/10.1016/j.electacta.2015.04.153.

(10) Galdikas, A.; Mironas, A.; Strazdien≐, V.; Šetkus, A.; Ancutien≐, I.; Janickis, V. Room-Temperature-Functioning Ammonia Sensor Based on Solid-State CuxS Films. *Sensors Actuators B Chem.* **2000**, *67* (1), 76–83. https://doi.org/10.1016/S0925-4005(00)00408-1.

(11) López De Mishima, B. A.; Lescano, D.; Molina Holgado, T.; Mishima, H. T.; De Mishima, B. A. L.; Lescano, D.; Holgado, T. M.; Mishima, H. T. Electrochemical Oxidation of Ammonia in Alkaline Solutions: Its Application to an Amperometric Sensor. *Electrochim. Acta* **1998**, *43* (3–4), 395–404. https://doi.org/10.1016/s0013-4686(97)00061-3.

(12) Ji, X.; Banks, C. E.; Compton, R. G. The Electrochemical Oxidation of Ammonia at Boron-Doped Diamond Electrodes Exhibits Analytically Useful Signals in Aqueous Solutions. *Analyst* **2005**, *130* (10), 1345–1347. https://doi.org/10.1039/b508975a.

(13) Vitse, F.; Cooper, M.; Botte, G. G. On the Use of Ammonia Electrolysis for Hydrogen Production. *J. Power Sources* **2005**, *142* (1–2), 18–26. https://doi.org/10.1016/j.jpowsour.2004.09.043.

(14) Li, Z. F.; Wang, Y.; Botte, G. G. Revisiting the Electrochemical Oxidation of Ammonia on Carbon-Supported Metal Nanoparticle Catalysts. *Electrochim. Acta* **2017**, *228*, 351–360. https://doi.org/10.1016/j.electacta.2017.01.020.

(15) Bunce, N. J.; Bejan, D. Mechanism of Electrochemical Oxidation of Ammonia. *Electrochim. Acta* **2011**, *56* (24), 8085–8093. https://doi.org/10.1016/j.electacta.2011.07.078.

(16) Johnston, S.; Suryanto, B. H. R.; MacFarlane, D. R. Electro-Oxidation of Ammonia on Electrochemically Roughened Platinum Electrodes. *Electrochim. Acta* **2019**, *297*, 778–783. https://doi.org/10.1016/j.electacta.2018.12.014.

(17) Wilhelm, T.; Biltz, A. The Fermentation of Nitrites and Nitrates by Electrolytic Oxidation of Ammonia in the Presence of Copper Hydroxide. *Berichte der Dtsch. Chem. Gesellschaft*

1904, *37*, 3130–3138.

(18) Gerischer, H.; Mauerer, A. Untersuchungen Zur Anodischen Oxidation von Ammoniak an Platin-Elektroden. *J. Electroanal. Chem.* **1970**, *25* (3), 421–433. https://doi.org/10.1016/S0022-0728(70)80103-6.

(19) de Vooys, A. C. A.; Koper, M. T. M.; Van Santen, R. A.; Van Veen, J. A. R. The Role of Adsorbates in the Electrochemical Oxidation of Ammonia on Noble and Transition Metal Electrodes. *J. Electroanal. Chem.* **2001**, *506* (2), 127–137. https://doi.org/10.1016/S0022-0728(01)00491-0.

(20) Corrigan, D. A. Effect of Coprecipitated Metal Ions on the Electrochemistry of Nickel Hydroxide Thin Films: Cyclic Voltammetry in 1M KOH. *J. Electrochem. Soc.* **1989**, *136* (3), 723. https://doi.org/10.1149/1.2096717.

(21) Shih, Y. J.; Huang, Y. H.; Huang, C. P. In-Situ Electrochemical Formation of Nickel Oxyhydroxide (NiOOH) on Metallic Nickel Foam Electrode for the Direct Oxidation of Ammonia in Aqueous Solution. *Electrochim. Acta* **2018**, *281*, 410–419. https://doi.org/10.1016/j.electacta.2018.05.169.

(22) Shih, Y. J.; Huang, Y. H.; Huang, C. P. Electrocatalytic Ammonia Oxidation over a Nickel Foam Electrode: Role of Ni(OH)2(s)-NiOOH(s) Nanocatalysts. *Electrochim. Acta* **2018**, *263*, 261–271. https://doi.org/10.1016/j.electacta.2018.01.045.

(23) Zahn, J. A.; Arciero, D. M.; Hooper, A. B.; DiSpirito, A. A. Evidence for an Iron Center in the Ammonia Monooxygenase from Nitrosomonas Europaea. *FEBS Lett.* **1996**, *397* (1), 35–38. https://doi.org/10.1016/S0014-5793(96)01116-7.

(24) Klinman, J. P. Mechanisms Whereby Mononuclear Copper Proteins Functionalize Organic Substrates. *Chem. Rev.* **1996**, *96* (7), 2541–2561. https://doi.org/10.1021/cr950047g.

(25) Herron, J. A.; Ferrin, P.; Mavrikakis, M. Electrocatalytic Oxidation of Ammonia on Transition-Metal Surfaces: A First-Principles Study. *J. Phys. Chem. C* **2015**, *119* (26), 14692–14701. https://doi.org/10.1021/jp512981f.

(26) Jiang, X.; Ying, D.; Liu, X.; Liu, M.; Zhou, S.; Guo, C.; Zhao, G.; Wang, Y.; Jia, J. Identification of the Role of Cu Site in Ni-Cu Hydroxide for Robust and High Selective Electrochemical Ammonia Oxidation to Nitrite. *Electrochim. Acta* **2020**, *345*, 136157. https://doi.org/10.1016/j.electacta.2020.136157.

(27) Licht, S. PH Measurement in Concentrated Alkaline Solutions. *Anal. Chem.* **1985**, *57* (2), 514–519. https://doi.org/10.1021/ac50001a045.

(28) Ambrose, J.; Barradas, R. G.; Shoesmith, D. W. Investigations of Copper in Aqueous Alkaline Solutions by Cyclic Voltammetry. *J. Electroanal. Chem.* **1973**, *47* (1), 47–64. https://doi.org/10.1016/S0022-0728(73)80344-4.

(29) Droog, J. M. M.; Alderliesten, C. A.; Alderliesten, P. T.; Bootsma, G. A. *Initial Stages of Anodic Oxidation of Polycrystalline Copper Electrodes in Alkaline Solution*; 1980; Vol. 111.

(30) Miller, B. Split-Ring Disk Study of the Anodic Processes at a Copper Electrode in Alkaline Solution. *J. Electrochem. Soc.* **1969**, *116* (12), 1675. https://doi.org/10.1149/1.2411657.

(31) Abd el Haleem, S. M.; Ateya, B. G. Cyclic Voltammetry of Copper in Sodium Hydroxide Solutions. *J. Electroanal. Chem.* **1981**, *117* (2), 309–319. https://doi.org/10.1016/S0022-

0728(81)80091-5.

(32) Deng, Y.; Handoko, A. D.; Du, Y.; Xi, S.; Yeo, B. S. In Situ Raman Spectroscopy of Copper and Copper Oxide Surfaces during Electrochemical Oxygen Evolution Reaction: Identification of CuIII Oxides as Catalytically Active Species. *ACS Catal.* **2016**, *6* (4), 2473–2481. https://doi.org/10.1021/acscatal.6b00205.

(33) Castro Luna De Medina, A. M.; Marchiano, S. L.; Arvía, A. J. The Potentiodynamic Behaviour of Copper in NaOH Solutions. *J. Appl. Electrochem.* **1978**, *8* (2), 121–134. https://doi.org/10.1007/BF00617670.

(34) McCafferty, E. *Introduction to Corrosion Science*; Springer New York, 2010. https://doi.org/10.1007/978-1-4419-0455-3.

(35) Davis, J.; Moorcroft, M. J.; Wilkins, S. J.; Compton, R. G.; Cardosi, M. F. Electrochemical Detection of Nitrate and Nitrite at a Copper Modified Electrode. *Analyst* **2000**, *125* (4), 737–741. https://doi.org/10.1039/a909762g.

(36) Savéant, J.; Costentin, C. *Elements of Molecular and Biomolecular Electrochemistry*; Wiley Online Library, 2019. https://doi.org/10.1002/9781119292364.

(37) Zhang, J.; Bond, A. M. Theoretical Studies of Large Amplitude Alternating Current Voltammetry for a Reversible Surface-Confined Electron Transfer Process Coupled to a Pseudo First-Order Electrocatalytic Process. *J. Electroanal. Chem.* **2007**, *600* (1), 23–34. https://doi.org/10.1016/j.jelechem.2006.02.023.

(38) Cuppett, J. D.; Duncan, S. E.; Dietrich, A. M. Evaluation of Copper Speciation and Water Quality Factors That Affect Aqueous Copper Tasting Response. *Chem. Senses* **2006**, *31* (7),

689–697. https://doi.org/10.1093/chemse/bjl010.

(39) Vidal-Iglesias, F. J.; Solla-Gullón, J.; Feliu, J. M.; Baltruschat, H.; Aldaz, A. DEMS Study of Ammonia Oxidation on Platinum Basal Planes. *J. Electroanal. Chem.* **2006**, *588* (2), 331–338. https://doi.org/10.1016/j.jelechem.2006.01.009.

(40) Endo, K.; Katayama, Y.; Miura, T. A Rotating Disk Electrode Study on the Ammonia Oxidation. *Electrochim. Acta* **2005**, *50* (11), 2181–2185. https://doi.org/10.1016/j.electacta.2004.09.024.

(41) Kumar, B.; Saha, S.; Ganguly, A.; Ganguli, A. K. A Facile Low Temperature (350 °c) Synthesis of Cu2O Nanoparticles and Their Electrocatalytic and Photocatalytic Properties. *RSC Adv.* **2014**, *4* (23), 12043–12049. https://doi.org/10.1039/c3ra46994h.